# Interannual and Seasonal Along-Shelf Current Variability and Dynamics: Seventeen Years of Observations from the Southern New England Inner Shelf

STEVEN J. LENTZ[a]

[a] *Physical Oceanography, Woods Hole Oceanographic Institution, Woods Hole, Massachusetts*

(Manuscript received 18 March 2022, in final form 4 July 2022)

ABSTRACT: The characteristics and dynamics of depth-average along-shelf currents at monthly and longer time scales are examined using 17 years of observations from the Martha's Vineyard Coastal Observatory on the southern New England inner shelf. Monthly averages of the depth-averaged along-shelf current are almost always westward, with the largest interannual variability in winter. There is a consistent annual cycle with westward currents of 5 cm $s^{-1}$ in summer decreasing to 1–2 cm $s^{-1}$ in winter. Both the annual cycle and interannual variability in the depth-average along-shelf current are predominantly driven by the along-shelf wind stress. In the absence of wind forcing, there is a westward flow of ~5 cm $s^{-1}$ throughout the year. At monthly time scales, the depth-average along-shelf momentum balance is primarily between the wind stress, surface gravity wave–enhanced bottom stress, and an opposing pressure gradient that sets up along the southern New England shelf in response to the wind. Surface gravity wave enhancement of bottom stress is substantial over the inner shelf and is essential to accurately estimating the bottom stress variation across the inner shelf.

SIGNIFICANCE STATEMENT: Seventeen years of observations from the Martha's Vineyard Coastal Observatory on the inner continental shelf of southern New England reveal that the depth-average along-shelf current is almost always westward and stronger in summer than in winter. Both the annual cycle and variations around the annual cycle are primarily driven by the along-shelf wind stress. The wind stress is opposed by a pressure gradient that sets up along the southern New England shelf and a surface gravity wave–enhanced bottom stress. The surface gravity wave enhancement of bottom stress is substantial in less than 30 m of water and is essential in determining the variation of the along-shelf current across the inner shelf.

KEYWORDS: Continental shelf/slope; Coastal flows; Momentum; Ocean dynamics; Wind stress

## 1. Introduction

Relatively little is known about the characteristics and dynamics of currents over continental shelves on monthly and longer times scales, primarily because current time series long enough to characterize seasonal and interannual variability are rare (e.g., Lentz 2008a). Currents over continental shelves tend to be primarily oriented along-shelf because of the coastal boundary and bathymetry constraints. Persistent along-shelf currents transport heat, salinity, and other constituents large distances along-shelf resulting in local water properties that are strongly influenced by upstream conditions (e.g., Chapman and Beardsley 1989; Loder et al. 1998; Lentz 2010; Shearman and Lentz 2010; Connolly and Lentz 2014). Consequently, low-frequency along-shelf currents are a key element in understanding the processes controlling interannual and seasonal variations over continental shelves.

Seventeen years of current profiles, meteorological forcing, and surface gravity wave characteristics collected at the Martha's Vineyard Coastal Observatory (MVCO) (Kirincich 2021) over the southern New England inner shelf (Fig. 1) provide a rare opportunity to examine the characteristics and dynamics of interannual and seasonal variability in the depth-average along-shelf current. At time scales from days to weeks, previous studies have found that along-shelf current variability over the southern New England inner shelf is primarily wind driven (Scott and Csanady 1976; Pettigrew 1981; Mayer 1982; Fewings and Lentz 2010; Kirincich 2013; Warner et al. 2014) and that the along-shelf wind stress is primarily balanced by bottom stress and an opposing along-shelf pressure gradient (Pettigrew 1981; Fewings and Lentz 2010)—a dynamical balance that is typical of many inner shelves (Lentz and Fewings 2012).

To place the MVCO observations in a broader cross-shelf context, time series from a 3-yr deployment of four mooring sites spanning the inner shelf (7–27-m water depth) are also analyzed (Fig. 1; Horwitz and Lentz 2014). After describing the observations and data processing (section 2) and estimation of terms in the depth-average along-shelf momentum balance (section 3), the seasonal and interannual variations in the depth-average current and its relationship to the local wind stress at monthly time scales are examined in section 4. The dynamical relationship between the wind stress and along-shelf current is then considered in the context of the depth-average momentum balance in sections 5a and 5b. The sea level response to the wind stress that results in an opposing along-shelf pressure gradient is examined in section 5c. Surface gravity wave enhancement of the bottom stress is an essential element of the dynamics and particularly the

Denotes content that is immediately available upon publication as open access.

*Corresponding author*: Steven J. Lentz, slentz@whoi.edu

DOI: 10.1175/JPO-D-22-0064.1

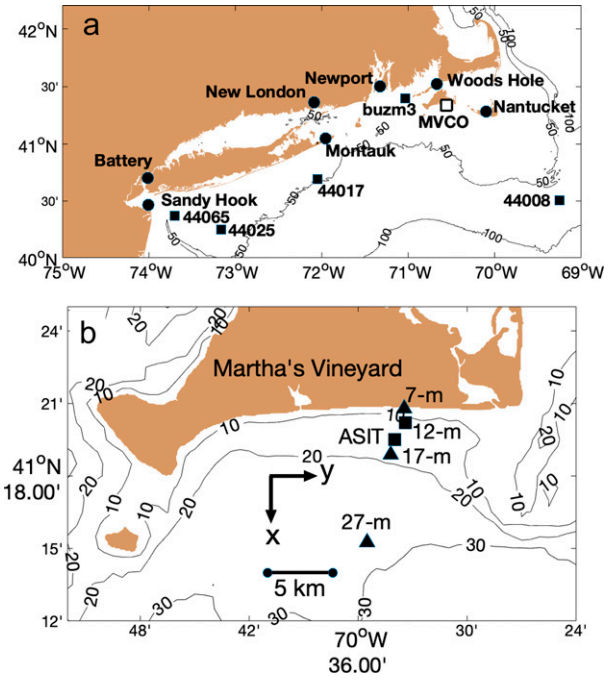


FIG. 1. (a) Map of southern New England showing location of MVCO, tide gauge stations (circles), and NDBC meteorological buoys (squares). (b) The inner shelf south of Martha's Vineyard showing 17-yr MVCO sites (squares) and 3-yr SWWIM measurement sites (triangles) and the coordinate frame.

variation in the along-shelf momentum balance across the inner shelf.

## 2. Observations and initial data processing

The MVCO includes a cabled underwater node 1.5 km offshore in 12 m of water supporting oceanographic instruments, an Air–Sea Interaction Tower (ASIT) 2.8 km offshore (Fig. 1b), and a meteorological tower on the beach (not shown). Measurements have been made at the 12-m site and the meteorological tower on the beach since 2001 and at ASIT since 2004.

This study focuses on current profiles from an upward-looking acoustic Doppler current profiler (ADCP) at the 12-m site from August 2001 to early September 2018. The ADCP sampled at 2 Hz with vertical bins every 0.5 m from 2.5 to 10 m above the bottom. Additionally, there are near-bottom pressure, water temperature, and salinity measurements at the 12-m site. Wind, air temperature, relative humidity, atmospheric pressure, and downward shortwave and longwave radiation are measured at the meteorological towers. Twenty-minute averages of the meteorological and oceanographic measurements, including surface gravity wave directional spectra estimated from the ADCP, were downloaded from the MVCO website (https://www.whoi.edu/mvco/).

Time series are also analyzed from a cross-shelf array of four mooring sites spanning the inner shelf at MVCO from October 2006 to February 2010 as part of the Stratification, Wind and Waves on the Inner Shelf (SWWIM) study (Fig. 1b; Horwitz and Lentz 2014). The mooring sites were in nominal water depths of 7 m (0.4 km offshore), 12 m (MVCO node 1.5 km offshore), 17 m (3.8 km offshore), and 27 m (11.1 km offshore). Each of the four sites included a bottom-mounted, upward-looking ADCP and a surface mooring supporting a chain of temperature (Onset Temp Pros) and temperature–conductivity (SeaBird MicroCATs) instruments spaced roughly every 2.5 m (temperature) and 5 m (conductivity) in the vertical direction.

Sea level measurements from NOAA tide gauges along the southern New England coast are used to estimate along-shelf pressure gradients (Fig. 1a). Meteorological measurements from NDBC buoys along the southern New England shelf are used to characterize spatial variations in wind stress and atmospheric pressure.

Depth-average currents are estimated by transforming the current profiles to a water-depth normalized uniform grid that spans approximately 0.2 (2.5 m above bottom) to 0.85 (10 m above bottom) and then, for simplicity, averaging the currents without extrapolating to the surface or bottom. Extrapolating to the surface and bottom did not significantly change the depth-average along-shelf currents.

Surface gravity wave Stokes drift velocities are estimated by integrating the 20-min wave directional spectra following Kenyon (1969). Lagrangian currents are then estimated as the sum of the measured Eulerian and estimated Stokes velocities. For the along-shelf currents focused on in this study, the depth-average Stokes velocities are small relative to depth-average Eulerian velocities, so the depth-average Eulerian and Lagrangian velocities are essentially the same. This is not the case for the depth-average cross-shelf currents (Lentz 2022).

Currents, near-bottom pressures, and sea levels are detided using T-Tide (Pawlowicz et al. 2002) prior to estimating monthly averages. Currents and winds are rotated into a coordinate frame aligned with the principal axes of the monthly depth-average Lagrangian currents. Cross-shelf ($x$) is positive offshore and along-shelf ($y$) is positive eastward, 94.5° clockwise from true north for the MVCO 12-m site (Fig. 1).

## 3. Depth-average momentum balance and estimation of terms

The depth-averaged along-shelf momentum balance may be written as

$$\rho h \frac{\partial v_{\mathrm{da}}^{L}}{\partial t} + \rho \frac{\partial}{\partial x} \int_{-h}^{\eta} (u^{L} v)\, dz + \rho h f u_{\mathrm{da}}^{L} = -\rho g h \frac{\partial \eta}{\partial y} + \tau^{sy} - \tau^{by}, \tag{1}$$

neglecting along-shelf variations in Eulerian and Stokes velocities (Connolly and Lentz 2021) and the along-shelf density gradient contribution to the pressure gradient (Fewings and Lentz 2010; also section 6a). Here $\rho$ is the water density (range from 1022.3 kg m$^{-3}$ in August to 1025.7 kg m$^{-3}$ in February); $h \approx 12$ m is the water depth; $v_{\mathrm{da}}^{L}$ and $u_{\mathrm{da}}^{L}$ are the depth-average along-shelf and cross-shelf Lagrangian velocity; $f = 0.96 \times 10^{-4}$ s$^{-1}$ is the Coriolis frequency; $g = 9.81$ m s$^{-2}$ is gravitational acceleration; $\eta$ is sea level plus atmospheric pressure (mean removed); and $\tau^{sy}$ and

$\tau^{by}$ are the along-shelf surface and bottom stresses. Outside the surf zone the along-isobath wave-radiation stress gradients are assumed to balance the bottom drag acting on the waves (Longuet-Higgins 2005) and consequently are not included in Eq. (1). Times when the 7-m SWWIM site was in the surf zone are excluded from the analysis—this occurred 3% of the time based on the criteria that the offshore wave height exceeds one-third of the water depth.

The acceleration term is estimated using a centered finite difference on the 20-min data. The nonlinear (second) term in Eq. (1) is estimated as a finite difference of the momentum flux between the 12-m site and the coast, where the cross-shelf momentum flux is zero. Connolly and Lentz (2021) note that this underestimates the convergence of momentum by a factor of 1.5 relative to estimates from the SWWIM moorings. Wind stress is estimate using the Coupled Ocean–Atmosphere Response Experiment (COARE) 3.5 bulk algorithm (Edson et al. 2013).

The along-shelf pressure gradient is estimated by a linear regression of sea level plus atmospheric pressure versus along-shelf distance using hourly data from seven tide gauges along the New England shelf, the near-bottom pressure at MVCO, and atmospheric pressure from the NDBC buoys interpolated to the tide gauge sites (Fig. 1). The decision to estimate the along-shelf pressure gradient from tides gauges spanning the entire southern New England shelf is based on several factors. The predominantly barotropic pressure response at monthly time scales is assumed to have large along-shelf scales (the length of the New England shelf is ~1000 km) so that the estimated pressure gradient is representative of the study region south of Martha's Vineyard. An empirical orthogonal function (EOF) analysis of the eight monthly sea level time series supports this assumption. The largest two modes account for 98.8% of the variance (94.35% for mode 1 and 4.46% for mode 2) and the modal structures are both linear with along-shelf distance from Nantucket to Sandy Hook. Use of pressure from all eight sites also reduces local anomalies associated with the particular location of individual tide gauge stations. Standard deviations of the along-shelf sea level gradient are $\sim 10^{-7}$ both from this analysis of monthly values and from daily values for the region south of Martha's Vineyard based using more accurate pressure gauges (Fewings and Lentz 2010). This implies that the pressure difference is 10 cm over 1000 km, but only 1 cm over 100 km, which is near the accuracy limit of tide gauges (e.g., Gobron et al. 2019; Lentz 1993). For these reasons, a linear regression using all eight sites to estimate the along-shelf pressure gradient yields better agreement with other terms in the along-shelf momentum balance than using sea level from two or three tide gauge stations in the vicinity of MVCO.

Bottom stress is estimated assuming a quadratic drag law $\tau^{by} = \rho C_D v_b \sqrt{(u_b^2 + v_b^2)}$ using the 20-min currents 2.5 m above the bottom. The time-dependent drag coefficient $C_D$ includes the influence of near-bottom surface gravity wave orbital velocities generating strong turbulence in the roughly centimeter-thick wave boundary layer (e.g., Grant and Madsen 1986). The $C_D$ is estimated using the formulation of Grant and Madsen (1979, 1986), the measured surface gravity wave height, period and direction, and an average hydrodynamic roughness, $z_o = 0.0014$ m, determined from direct covariance stress estimates by Scully et al. (2018) for a site 3 km from the MVCO 12-m ADCP. This $z_o$ is associated with sand ripples and is substantially larger than the $z_o = 1.2 \times 10^{-4}$ m used by Fewings and Lentz (2010), and consequently, the drag coefficient is about 2 times as large. To determine the importance of surface gravity wave enhancement at monthly time scales, bottom stress is also estimated using a constant drag coefficient $C_D = 0.0029$ based on $z_o = 0.0014$ m and the height of the lowest ADCP bin. For monthly averages, accounting for surface gravity waves results in a bottom stress that is, on average, about 2 times the magnitude of the constant $C_D$ bottom stress at the 12-m site.

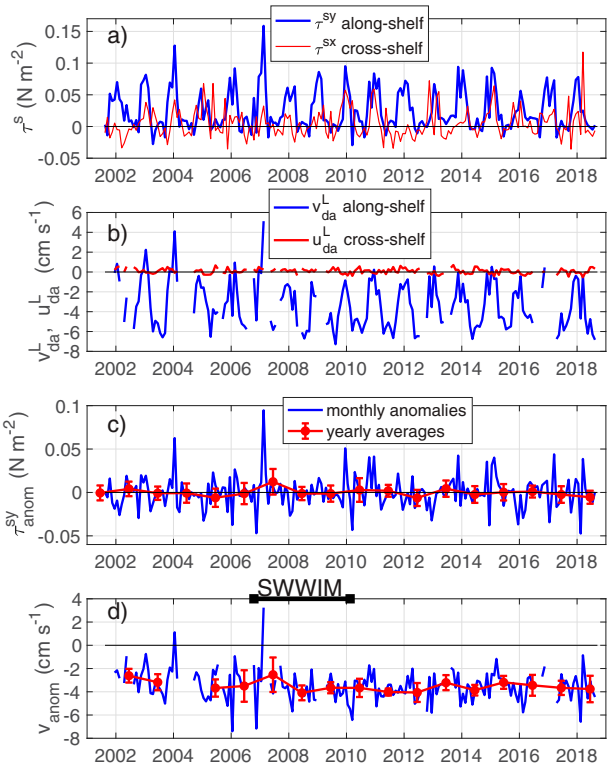


FIG. 2. Time series of monthly averages of (a) wind stress at MVCO Air–Sea Interaction Tower, (b) depth-average currents at the MVCO 12-m site, and anomalies relative to annual cycle of the (c) along-shelf wind stress and (d) depth-average along-shelf current. Yearly averages in (c) and (d) include 95% confidence intervals based on standard error of the means. The time period of SWWIM deployments is also indicated. Along-shelf is positive eastward, and cross-shelf is positive offshore.

## 4. Overview of wind stress and depth-average along-shelf current

### a. *Wind stress and stratification*

Monthly wind stresses are not strongly polarized, but the largest wind stresses tend to be offshore and toward the east (Fig. 2a). Along-shelf wind stresses exhibit a consistent annual cycle with eastward wind stresses (~0.05 N m$^2$) in autumn and winter (October–March) and weak wind stresses (<0.02 N m$^2$)

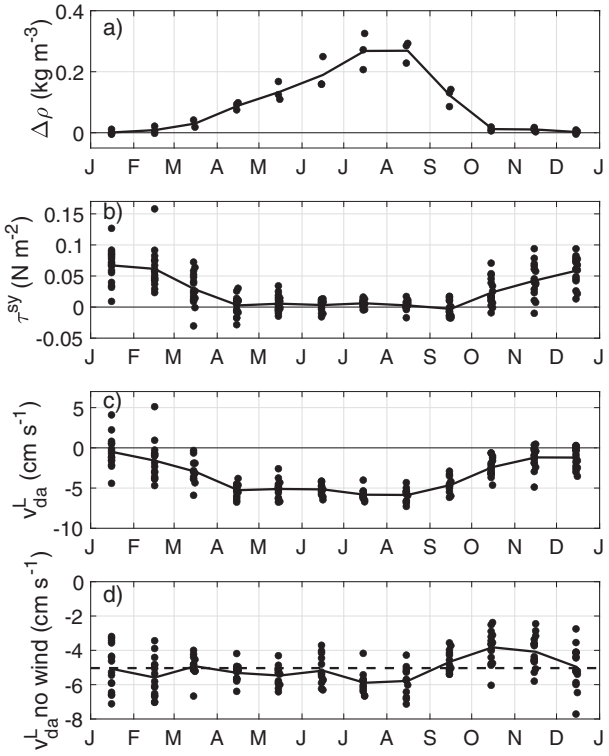


FIG. 3. Monthly averages (circles) and average annual cycle (line) of (a) the density difference between 0.9 and 11 m above the bottom at the 12-m site (from 3-yr SWWIM deployment), (b) the along-shelf wind stress (positive eastward), (c) the depth-average along-shelf current (positive eastward) at the 12-m site, and (d) the depth-average current after removing the linear local wind-driven response (the dashed line is the mean residual current). Annual cycle standard error of the means range from 0.001 to 0.003 N m$^{-2}$ and from 2 to 3 mm s$^{-1}$ in summer and from 0.006 to 0.008 N m$^{-2}$ and from 5 to 6 mm s$^{-1}$ in winter.

in spring and summer (April–September) (Fig. 3b). Year-to-year variations in along-shelf wind stresses are larger in winter than summer (Fig. 3b), with anomalously strong eastward wind stresses associated with winter storms in January 2004 and February 2007 (Fig. 2a). These characteristics of the monthly wind stresses at MVCO are representative of the entire southern New England shelf (Lentz 2008b), since the scale of the wind forcing is larger than the extent of southern New England shelf. Monthly along-shelf wind stresses from the NDBC buoys over the southern New England shelf (Fig. 1) are highly correlated (0.93–0.96) with the MVCO wind stress, but wind stress magnitudes are about 40% larger over the midshelf than at the MVCO inner-shelf site.

At the 12-m site, density stratification is weak, nearly zero, during the winter and stronger during the summer (Fig. 3a). Based on the annual cycles of the wind stress and stratification two "seasons" are defined, winter is October–March and summer is April–September.

### b. *Depth-averaged along-shelf currents*

Monthly depth-average currents are strongly polarized along-shelf (Fig. 2b), in contrast to the wind stress (Fig. 2a). The monthly depth-average along-shelf currents at the 12-m site are westward 93% of the time, typically ranging between 0 and −7 cm s$^{-1}$, with anomalous eastward currents exceeding 4 cm s$^{-1}$ in the winters of 2004 and 2007 when eastward wind stresses are also anomalously strong (>0.1 N m$^{-2}$, Figs. 2b,a). There is a clear annual cycle in the depth-average along-shelf current with a relatively constant westward flow of 5 cm s$^{-1}$ in summer and a weaker westward flow of 1–3 cm s$^{-1}$ in winter (Fig. 3c).

Along-shelf wind stress and depth-average current anomalies, relative to the annual cycle, tend to be smaller than the annual cycle with a few notable exceptions (Figs. 2c,d). The monthly current anomalies have a standard deviation of 1.3 cm s$^{-1}$ and a range of −7.4 to 3.2 cm s$^{-1}$ (Fig. 2d). Current anomalies are larger prior to 2007 than after, when the range of month-to-month variations is ±2 cm s$^{-1}$ about the mean. A similar pattern of anomaly variability is evident in the along-shelf wind stress (Fig. 2c). Month-to-month variations in the depth-average along-shelf current are 2 times as large in winter as in summer (standard deviations 1.8 vs 0.9 cm s$^{-1}$; Fig. 3c). Year-to-year variations are relatively small, ranging from −2.5 to −4.1 cm s$^{-1}$, with a standard deviation of 0.5 cm s$^{-1}$ (Fig. 2d, red line). Notably, there is not a significant trend in the yearly values or obvious multiyear variability, though there is a hint of weaker yearly average currents in 2002–03.

The 3-yr SWWIM array time series suggest that monthly depth-average along-shelf current variability at the 12-m site is representative of the inner-shelf from the 7- to the 27-m isobath. Correlations between along-shelf currents at the four sites are all greater than 0.89 (all correlations in the following analyses are significantly different from zero at the 95% confidence level unless noted otherwise). Regression slopes (with 95% confidence intervals), relative to the 12-m site, are 2.0 ± 0.5 for the 27-m site, 0.95 ± 0.1 for the 17-m site, and 1.3 ± 0.2 the 7-m site. It will be shown in section 5b that the variation across the inner shelf in the strength of the monthly depth-average along-shelf current variability is due to cross-shelf variations in the relative strength of the bottom stress and pressure gradient terms in Eq. (1).

### c. *Wind response*

The depth-average along-shelf current is correlated with the along-shelf wind stress. The correlation between $\tau^{sy}$ and $v^L_{da}$ at the 12-m site is 0.86 (0.89 for the wind stress component along 120° clockwise from true north). Thus, the wind stress accounts for 74% [79% wind stress oriented 120° at true north (T)] of the monthly depth-average along-shelf current variance. The regression slope is 0.63 ± 0.05 m s$^{-1}$ N$^{-1}$ m$^{-2}$ and the intercept is 5.0 ± 0.2 cm s$^{-1}$. Removing the annual cycle from both the wind stress and depth-average current (Figs. 2c,d), the maximum correlation is 0.70 (0.76 wind stress oriented 120°T) and the regression slope is 0.46 ± 0.07 m s$^{-1}$ N$^{-1}$ m$^{-2}$. The wind stress also accounts for one-half of the variance in the yearly averages, with a correlation of 0.72 and a regression slope of 0.72 ± 0.40 m s$^{-1}$ N$^{-1}$ m$^{-2}$ (16 yearly values) (Figs. 2c,d, red lines). The relationship between $\tau^s$ and $v^L_{da}$ for monthly averages is similar to the relationship for daily averages with or

without the annual cycle (e.g., maximum correlation 0.82; regression slope 0.53 ± 0.01 m $s^{-1}$ $N^{-1}$ $m^{-2}$ for daily values with annual cycle).

The residual of the depth-average along-shelf current after removing the linear wind-driven response has a mean of −5.0 cm $s^{-1}$ and a standard deviation of 1.1 cm $s^{-1}$ (Fig. 3d). In contrast to the wind-driven response, the residual does not exhibit an obvious annual cycle, though there is on average a slightly weaker westward flow in autumn (October–November) relative to the rest of the year. The wind stress also accounts for the largest anomalies in the depth-average along-shelf current seen in Fig. 2d. Removing the linear wind-driven response reduces the range about the mean from a range from −3.9 to 6.7 cm $s^{-1}$ to a range from −2.2 to 2.1 cm $s^{-1}$. Note the local wind stress does not account for the consistent ~5 cm $s^{-1}$ westward along-shelf current (Fig. 3d).

In summary, the linear regression analysis establishes that a majority of the along-shelf current variance is related to the along-shelf wind stress and provides a simple basis for comparisons at different time scales and with other coastal sites. However, a key point of this study is that the dynamical relationship is more complex than the wind stress directly forcing the along-shelf current. It will be shown in section 5 that the wind stress is not only balanced by the local bottom stress, but also sets up an opposing along-shelf pressure gradient that reduces the effectiveness of wind stress in forcing an along-shelf current.

## 5. Along-shelf momentum balance

To determine the dynamical relationship between the wind stress and the depth-average along-shelf current, the depth-average along-shelf momentum balance [Eq. (1); section 3] at monthly time scales is examined focusing initially on the 17-yr time series at the 12-m site and then on variations across the inner shelf using the 3-yr time series from SWWIM.

### *a. 12-m site (MVCO)*

At monthly time scales the largest estimated terms in the depth-average along-shelf momentum balance Eq. (1) are the wind stress, the barotropic pressure gradient, and the bottom stress (Table 1). The means and standard deviations of the acceleration, nonlinear cross-shelf flux of along-shelf momentum, and the Coriolis terms are less than 10% of the wind stress. Inclusion of these smaller terms does not improve the closure of the momentum balance at monthly time scales.

The focus here is on the dynamics of the monthly variability, in part because the mean along-shelf pressure gradient cannot be accurately estimated from the tide gauge data. However, the wind stress and bottom stress means are as large as the standard deviations (Table 1). The mean wind stress and bottom stress are approximately the same magnitude but have opposite signs and hence do not balance because the mean wind stress is eastward and the mean along-shelf current is westward. This implies that the sum must be balanced by a mean along-shelf pressure gradient or other body force. A mean along-shelf sea level gradient of $\partial\eta/\partial y = 4.5 \times 10^{-7}$ would be required to balance the sum of the mean wind stress and bottom stress, and drive the observed mean westward flow in the absence of wind forcing (Fig. 3d). This is similar to a recent estimate for this site of $\partial\eta/\partial y = 3.9 \times 10^{-7}$, based on covariance stress estimates from the MVCO ADCP (Kirincich 2013), but more than 2 times as large as two other estimates (Lentz 2008a; Fewings and Lentz 2010).

TABLE 1. Means and standard deviations of estimated terms in the vertically integrated along-shelf momentum balance for 168 months ($10^{-2}$ N $m^{-2}$).

| Term | Mean | Std dev | |
|---|---|---|---|
| | | Monthly | Daily |
| $\tau^{sy}$ | 2.7 | 3.2 | 9.1 |
| $\rho g h \partial\eta/\partial y$ | — | 1.5 | 3.3 |
| $\tau^{by}$ | −2.8 | 2.2 | 7.3 |
| $\rho h \partial v_{da}/\partial t$ | 0.0 | 0.1 | 1.4 |
| $\rho\partial(\int uv\,dz)/\partial x$ | 0.0 | 0.1 | 0.2 |
| $\rho f h u^{L}_{da}$ | 0.1 | 0.3 | 1.0 |
| Residual | 5.4 | 1.6 | 4.5 |

At the 12-m site, the standard deviation of the along-shelf pressure gradient and bottom stress terms are, respectively, one-half and two-thirds of the wind stress (Table 1). The standard deviation of the sum of the along-shelf pressure gradient and bottom stress terms, $3.3 \times 10^{-2}$ N $m^{-2}$, is similar to the standard deviation of the wind stress, $3.2 \times 10^{-2}$ N $m^{-2}$. The monthly variations in the along-shelf pressure gradient and bottom stress are both correlated with the wind stress (correlations 0.86 and 0.77) with regression slopes less than 1 (Figs. 4a,b). The sum of the pressure gradient and bottom stress terms tends to balance the wind stress—correlation 0.89 and a regression slope of 0.91 ± 0.07 (Fig. 4c). A multiple regression analysis ($\tau^{sy} = a\partial P/\partial y + b\tau^{by} + c$) does not substantially improve the correlation (0.91), indicating the estimates of the pressure gradient and bottom stress terms are reasonable. Assuming a constant $C_D$, that is, no wave enhancement of the bottom stress, yields a similar correlation (0.92) between the wind stress and the sum of the pressure gradient and bottom stress, but with a regression slope, 0.71 ± 0.05, that is significantly less than 1.0.

Although dominated by the stronger wind stress variability in winter, these dynamical relationships are similar in winter and summer (Fig. 4, blue and red circles). The wind stress accounts for essentially all of the annual cycle (94% of the variance) in the sum of the along-shelf pressure gradient and bottom stress and for most of the variance (correlation 0.8) in the monthly anomalies about the annual cycle (regression slope 0.97 ± 0.11). For the 16 yearly averages, the variability in the dominant terms is smaller than for monthly averages (15%–30% of the monthly standard deviations). However, at yearly time scales there is still a significant correlation between the along-shelf wind stress and the sum of the along-shelf pressure gradient and bottom stress (correlation 0.60; regression slope 1.2 ± 0.9). Thus, at monthly or yearly time scales, the along-shelf wind stress is balanced by an opposing

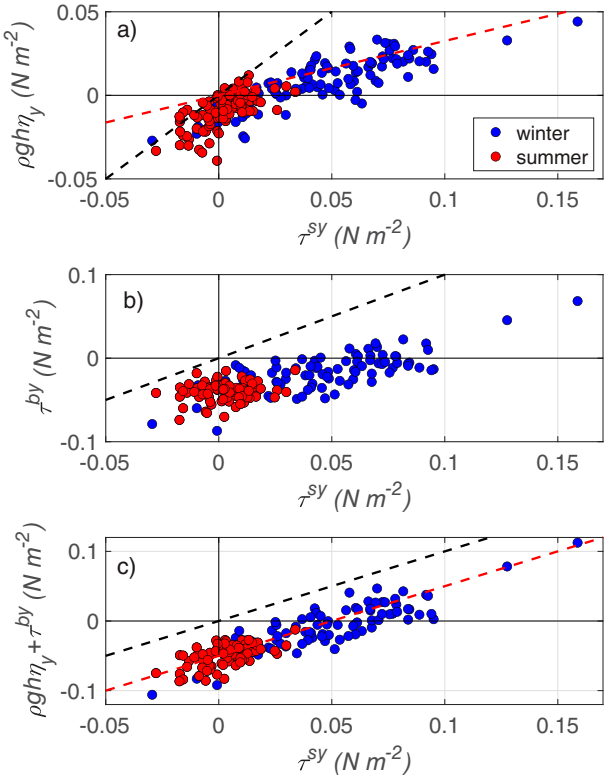


FIG. 4. Wind stress dependence of (a) the along-shelf pressure gradient term, (b) bottom stress, and (c) their sum. The black dashed lines have a slope of 1 and an intercept of 0. In (a) the red dashed line is the predicted relationship from the ATW model [Eq. (3); section 5c] for the along-shelf location midway along the southern New England shelf ($y = -190$ km); the coefficient in Eq. (3) has been multiplied by 1.4 to account for MVCO wind stress being weaker than the midshelf wind stress. In (c) the red dashed line has an intercept corresponding to a mean along-shelf sea level gradient of $\partial\eta/\partial y = 4.5 \times 10^{-7}$ that is not related to the local wind stress.

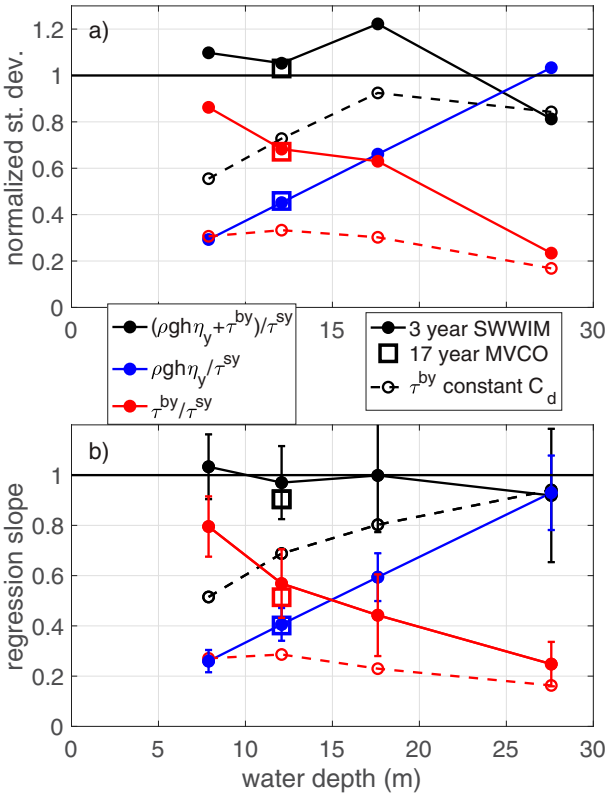


FIG. 5. Cross-shelf variation in depth-average along-shelf momentum balance (a) standard deviation of dominant terms normalized by standard deviation of the wind stress and (b) linear regression slope between wind stress and other dominant terms. Dashed lines show results for a constant drag coefficient bottom stress estimate.

pressure gradient and a surface gravity wave–enhanced bottom stress.

### b. *Variation across inner shelf (SWWIM)*

Assuming the wind stress and the along-shelf pressure gradient do not vary substantially across the inner shelf, the three dominant terms in the along-shelf momentum balance Eq. (1) indicate that as the water depth increases the bottom stress should decrease to compensate for the increase in the pressure gradient term. Estimates from the four SWWIM sites support this hypothesis. Standard deviations of the bottom stress decrease (Fig. 5a, red line) at about the same rate that the pressure gradient term increases with water depth (Fig. 5a, blue line) such that the standard deviation of the sum of the pressure gradient and bottom stress is relatively constant (Fig. 5a, black line with circles) and approximately equal to the wind stress standard deviation at all four sites.

The linear regression slopes exhibit the same pattern (Fig. 5b). As the water depth increases, regression slopes between the wind stress and bottom stress decrease at about the same rate as the regression slopes between the wind stress and pressure gradient term increase (Fig. 5b, red and blue lines). Consequently, the regression slope between the wind stress and the sum of the pressure gradient and bottom stress is approximately equal to 1 across the inner shelf (black line with circles in Fig. 5b). The corresponding correlations range from 0.86 to 0.97. The standard deviations and regression slopes indicate that the bottom stress and along-shelf pressure gradient have similar magnitudes in about 15 m of water. In 7 m of water the wind stress is predominantly balanced by the bottom stress, whereas in 27 m of water the wind stress is predominantly balanced by the along-shelf pressure gradient. The standard deviations and linear regression slopes from the 12-m site during the 3-yr SWWIM study are similar to the values from the 17-yr time series (Fig. 5, squares), suggesting that the relatively short SWWIM study is representative of the relationships over longer time scales.

Constant $C_D$ bottom stress estimates (Fig. 5, dashed lines) do not account for the variation across the inner shelf as well as the bottom stress estimates that include surface gravity wave enhancement. Standard deviations of the constant $C_D$ bottom stress do not vary substantially as the water depth increases from 7 to 27 m and consequently do not balance the

increase in the pressure gradient term (Fig. 5a). The same pattern is evident in the regression slopes. The regression slope between the wind stress and the sum of the pressure gradient and constant $C_D$ bottom stress decreases by nearly a factor of 2 from the 27-m site to the 7-m site (Fig. 5b, black dashed line) rather than remaining constant at about 1, as seen for the wave-enhanced bottom stress (black solid line). The difference between the wave-enhanced and constant $C_D$ bottom stress standard deviations decreases as the water depth increases (Fig. 5a, red lines), indicating that on monthly time scales surface wave enhancement of the bottom stress primarily occurs onshore of the 30-m isobath at this location. The cross-shelf variation in the along-shelf momentum balance demonstrates the importance of the surface gravity wave enhancement of bottom stress over the inner shelf.

### c. *Sea level response to wind stress: Setup of along-shelf pressure gradient*

The examination of the along-shelf momentum balance in the two previous sections establishes the importance of the along-shelf pressure gradient that opposes the wind stress but does not address the dynamics that set up the along-shelf pressure gradient over the southern New England shelf. Linear regression slopes between the along-shelf wind stress at midshelf (NDBC 44017; Fig. 1) and sea level (including atmospheric pressure) at the seven tide gauge stations and MVCO increases from $-0.5$ m N$^{-1}$ m$^{-2}$ at Nantucket to $-1.5$ m N$^{-1}$ m$^{-2}$ at Sandy Hook (Fig. 6). The corresponding correlation magnitudes increase from 0.4 at Nantucket to 0.8 at Sandy Hook/Battery. The negative regression slopes imply that an eastward (positive) along-shelf wind stress (upwelling favorable) causes a setdown of sea level at the coast, as expected. This tendency for the wind-driven sea level response to be weaker at Nantucket relative to Sandy Hook was previously noted by Wang (1979). An obvious consequence of this relationship is that there is an along-shelf sea level gradient that opposes the along-shelf wind stress.

Qualitatively, an eastward (positive) wind stress along the southern New England shelf forces an offshore Ekman transport in the surface boundary layer that causes a setdown of sea level at the coast that ultimately accelerates an eastward (westward) along-shelf current in geostrophic balance with the cross-shelf pressure gradient. East of Nantucket (Fig. 1), there is not an east–west coastal boundary to block the cross-wind Ekman transport and consequently there is no setdown and hence no along-shelf current. Because long coastal-trapped waves propagate with the coast on the right (Northern Hemisphere), the along-shelf current and the associated coastal setdown increase toward the west (Sandy Hook; Fig. 1). This implies that east–west along-shelf wind stresses drive an along-shelf sea level gradient that opposes the wind stress, with smaller sea level variations at Nantucket relative to Sandy Hook as observed (Fig. 6).

This qualitative description of the response is quantified in the steady, linear, arrested topographic wave (ATW) model proposed by Csanady (1978). The model assumes a steady, barotropic, depth-average flow, with a geostrophic cross-shelf

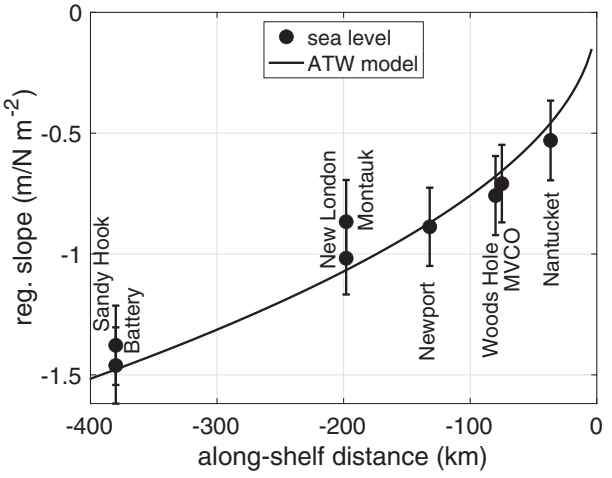


FIG. 6. Linear regression slope between a midshelf wind stress (buoy 44017) and the sea level (including atmospheric pressure) ($\eta = a\tau^{sy} + b$) for eight tide gauge/pressure stations along the southern New England shelf (Fig. 1). The predicted relationship from the ATW model (Csanady 1978) is also shown. For the midshelf wind stress, the along-shelf component is parallel to the southern New England coast (80° clockwise from true north). Error bars on regression slopes are 95% confidence intervals. Along-shelf distances are relative to the western edge of Great South Channel.

momentum balance and a linear along-shelf momentum balance that also assumes a linear drag law relating the bottom stress to the depth-average current. The sea level response at the coast forced by a constant along-shelf wind stress over a finite stretch of coast (southern New England shelf) is

$$\eta(\tilde{x} = 0) = -\frac{2}{\sqrt{\pi}}\frac{\tau^{sy}}{\rho g}\left(\frac{-fy}{r\partial h/\partial x}\right)^{1/2} \tag{2}$$

in the region of constant wind forcing [Eq. (24) and Fig. 5 in Csanady (1978)]. Here $y$ is the distance along-shelf from where the wind forcing begins (negative in this case). Taking the onset of the wind forcing at the western edge of the Great South Channel (Fig. 1), the average bottom slope over the New England shelf $\partial h/\partial x = 0.6 \times 10^{-3}$ (Lentz 2008a), and an optimal linear drag coefficient of $r = 3.5 \times 10^{-4}$ m s$^{-1}$ reproduces the observed sea level response to along-shelf wind stress on the southern New England shelf (Fig. 6, line; see also Noble et al. 1983). The optimal linear drag coefficient is similar to previous estimates for the Middle Atlantic Bight (e.g., Lentz 2008a; $r = 2.5 \times 10^{-4}$ m s$^{-1}$). Taking the $y$ derivative of Eq. (2) provides an estimate of the along-shelf pressure gradient

$$\frac{\partial \eta(\tilde{x} = 0)}{\partial y} = -\frac{1}{\sqrt{\pi}}\frac{\tau^{sy}}{\rho g}\left(\frac{f}{r\partial h/\partial x}\right)^{1/2}(-y)^{-1/2} \tag{3}$$

(note that there is a singularity at $y = 0$ due to the abrupt onset of the wind stress). Choosing $y = -190$ km (halfway between $y = 0$ and Sandy Hook), Eq. (3) provides an accurate estimate of the regression slope between the MVCO wind

stress and the estimate pressure gradient along the southern New England shelf (Fig. 4a, red dashed line). [The relationship from Eq. (3) has been multiplied by 1.4 in Fig. 4a, the regression coefficient relating the weaker wind stress at MVCO to the midshelf wind stress.] The along-shelf pressure gradient is part of the shelf-wide response to the wind and therefore depends on the midshelf wind stress, bottom slope, and drag coefficient and not on the inner-shelf values. In summary, the opposing along-shelf pressure gradient is a consequence of the sea level response to along-shelf wind stresses over the finite extent of the southern New England shelf. A detailed examination of the wind-driven sea level response along the entire Middle Atlantic Bight coast is the subject of ongoing research.

## 6. Discussion

### a. *Along-shelf momentum balance residual and uncertainties*

While there is a strong tendency for the along-shelf pressure gradient and bottom stress to balance the wind stress (section 5), the standard deviation of the residual in the along-shelf momentum balance is half the size of the wind stress and much larger than the neglected acceleration, Coriolis, and cross-shelf momentum flux convergence terms (Table 1). The residual could be due to two terms in the along-shelf momentum balance that could not be estimated, the along-shelf buoyancy gradient contribution to the pressure gradient, and the along-shelf momentum flux convergence/divergence. Daily estimates of these two terms were made using observations from a shorter, 7-month deployment, of an array of current profilers and density chains extending 20 km along the 15-m isobath south of Martha's Vineyard (Kirincich and Lentz 2017). The standard deviation of the daily along-shelf momentum flux is ~15% of the wind stress. The buoyancy gradient term is 50% of the wind stress in summer, but only 10% in winter, suggesting it could be a significant contribution to the residual at monthly time scales in summer. Coastal radar measurements of surface currents and high-resolution numerical models indicate that tidal rectification is substantial south of Martha's Vineyard and consequently may contribute to monthly variability in the along-shelf currents and dynamics (Ganju et al. 2011; Kirincich et al. 2013).

The difference in the along-shelf scales of the pressure gradient and bottom stress estimates is undoubtedly a major factor contributing to the residual. The pressure gradient estimate is an average over the 400-km extent of the southern New England coast whereas the bottom stress is a point measurement. There are likely to be differences in the monthly bottom stress along the southern New England inner shelf as the tidal currents decrease substantially from east to west (Moody et al. 1983; Shearman and Lentz 2004) and the surface gravity wave characteristics probably vary as well given the along-shelf variations in bathymetry. The tendency for the large-scale pressure gradient and the bottom stress to balance the wind stress (Figs. 4c and 5b) suggests the MVCO bottom stress variability at monthly time scales is representative of the bottom stress over the extent of the southern New England inner shelf. However, there are not simultaneous long-term measurements to directly test this assumption.

The larger-scale pressure gradient estimate does not resolve shorter-scale variability in the along-shelf pressure gradient in the vicinity of MVCO associated with the island of Martha's Vineyard and the complex local bathymetry (Fig. 1), residuals from the strong tidal currents in the area (e.g., Kirincich et al. 2013), and other processes. For the reasons discussed in section 3, using two or three tide gauges in the vicinity of MVCO to include shorter-scale variability resulted in poorer agreement with other terms in the along-shelf momentum balance than using eight sites that spanned the southern New England shelf. Arrays of more accurate pressure gauges were deployed south of Martha's Vineyard for 2.5 months in 2001 (pressure gauges 37 km apart on ~20-m isobath) and 3 months in 2003 (pressure gauges 13.9 km apart on the 15-m isobath) (Fewings and Lentz 2010). Daily averages of the local detided along-shelf pressure gradient estimated from these pressure sensors are correlated with the larger-scale tide gauge estimates, with a correlation of 0.75 for 2001 and 0.58 for 2003, with regression slopes of $0.67 \pm 0.23$ and $1.24 \pm 0.17$, respectively. These comparisons indicate the larger-scale tide gauge estimates are to some extent representative of the local along-shelf pressure gradient, but the causes of the differences at daily time scales are uncertain, as is the relationship between daily and monthly time scales.

### b. *Relationship to daily time scales and previous studies*

The tendency for the along-shelf wind stress, pressure gradient, and bottom stress to be the dominant terms and to balance at monthly time scales is consistent with results at daily time scales. Standard deviations of the terms for daily averages are about 3 times as large as for monthly averages and the smaller terms are more substantial, particularly the along-shelf acceleration (Table 1). The correlation between daily values of the along-shelf wind stress and the sum of the along-shelf pressure gradient and bottom stress is 0.87 versus 0.89 for monthly values, and the regression slopes are similar. Correlations and regression slopes between the wind stress and either the pressure gradient or bottom stress are also similar for monthly and daily values.

Previous studies indicate that at daily time scales over inner shelves there is generally a balance between the along-shelf wind stress, pressure gradient, and bottom stress (Lentz and Fewings 2012; Lee et al. 1984, 1989; Lentz and Winant 1986; Lentz 1994; Lentz et al. 1999; Liu and Weisberg 2005; Gutierrez et al. 2006; Kirincich and Barth 2009), including the southern New England inner shelf (Scott and Csanady 1976; Pettigrew 1981; Fewings and Lentz 2010; Kirincich 2013). At monthly and longer time scales, and associated larger along-shelf scales, this three term balance is likely to be more dominant. As observed in this study at monthly time scales, the along-shelf pressure gradient is correlated with and opposes the local wind stress at daily time scales at several inner shelf sites (e.g., Lentz 1994; Yankovsky and Garvine 1998; Liu and Weisberg 2005; Kirincich and Barth 2009), including the southern New England inner shelf (Pettigrew 1981; Fewings and Lentz 2010).

### c. *Bottom stress*

This study provides compelling evidence that surface gravity waves have a substantial impact on the bottom stress acting on the subtidal flow and on the variation in bottom stress across the inner shelf. This is consistent with a previous study focusing on the momentum balance at daily time scales at this site (Fewings and Lentz 2010). Surface gravity wave enhancement of the bottom stress is likely to be important on most inner shelves but is rarely considered in studies of the momentum balance or in numerical models (Lentz and Fewings 2012). This study neglects a number of other factors that are likely to impact the bottom stress, including evolution of bed forms (sand ripples) and the relative orientations of the bedforms, surface gravity wave orbital velocities, and lower-frequency (relative to wave time scales) near-bottom currents (e.g., Wiberg and Harris 1994; Grant and Madsen 1986; Trowbridge and Lentz 2018; Scully et al. 2018). This study also assumed that the hydrodynamic roughness estimate near the 12-m site was representative of the hydrodynamic roughness at the other SWWIM sites, which is probably not accurate given variations in the dominant grain size and bed forms across the inner shelf (Goff et al. 2005). A major challenge for accurately modeling inner-shelf circulation is developing a better understanding of bottom stress in the presence of surface gravity waves and a moveable seabed (Trowbridge and Lentz 2018).

## 7. Summary

Monthly to yearly depth-average along-shelf current variations are examined using 17 years of observations from the Martha's Vineyard Coastal Observatory 12-m site on the southern New England inner shelf. Monthly depth-averaged along-shelf currents at the 12-m site are almost always westward, except during a couple winter months with anomalously strong eastward wind stresses (Figs. 2a,b). The monthly along-shelf current variability consists primarily of a mean plus annual cycle with a current of $-5$ cm s$^{-1}$ (westward) in summer (April–September) decreasing in magnitude to $-1$ cm s$^{-1}$ (westward) in winter (November–February) (Fig. 3c). Month-to-month variations about the annual cycle range from $-7.4$ to 3.2 cm s$^{-1}$ (Fig. 2d, blue line). Year-to-year variations range from $-4.1$ to $-2.5$ cm s$^{-1}$, without a significant trend or obvious multiyear variability (Fig. 2d, red line).

The along-shelf wind stress accounts for most of the variance in the monthly depth-average along-shelf current, including the annual cycle (Fig. 3c), and at least one-half of the month-to-month and year-to-year variability about the annual cycle (Fig. 2d). In the absence of local wind forcing, the depth-average along-shelf current is westward at $\sim 5 \pm 2.5$ cm s$^{-1}$ without an annual cycle (Fig. 3d).

The dominant terms in the along-shelf momentum balance are the wind stress, the bottom stress, and an along-shelf pressure gradient that opposes the wind stress (Table 1). A key element of the bottom stress is enhancement by surface gravity waves. The opposing along-shelf pressure gradient sets up along the southern New England shelf in response to the local along-shelf wind stress and consistent with the arrested topographic wave model proposed by Csanady (1978) (Figs. 6 and 4a). The along-shelf pressure gradient and bottom stress are both correlated with the wind stress (Figs. 4a,b) and their sum tends to balance the wind stress (Fig. 4c). Measurements from a 3-yr deployment of a cross-shelf array of four mooring sites in 7, 12, 17, and 27 m of water indicate that the bottom stress term decreases offshore at the same rate that the pressure gradient term increases offshore provided the bottom stress estimate includes surface gravity wave enhancement (Fig. 5). The balance is primarily between the wind stress and bottom stress in 7 m of water and between the wind stress and pressure gradient in 27 m of water (Fig. 5). This result emphasizes the importance of surface gravity waves to the variation in bottom stress across the inner shelf and hence to the cross-shelf structure of the along-shelf current.

*Acknowledgments.* This study is possible because of all the people that contributed to the Martha's Vineyard Coastal Observatory, including deploying and maintaining the instrumentation and processing and archiving the resulting data. Thanks are given to Anthony Kirincich, Ken Brink, Melanie Fewings, and three anonymous reviewers for numerous suggestions that substantially improved this paper. The National Science Foundation, Woods Hole Oceanographic Institution, the Massachusetts Technology Collaborative, and the Office of Naval Research have supported the construction and maintenance of MVCO. The analysis presented here was partially funded by the National Science Foundation under Grants OCE 1558874 and OCE 1655686.

*Data availability statement.* The MVCO data are available at https://mvco.whoi.edu. The Stratification, Wind and Waves on the Inner shelf of Martha's Vineyard (SWWIM) data are available at https://hdl.handle.net/1912/27252. The NDBC meteorological data are available at https://www.ndbc.noaa.gov. The NOAA tide gauge data are available at https://tidesandcurrents.noaa.gov/stations.html?type=Historic±Water±Levels.

## REFERENCES

Chapman, D. C., and R. C. Beardsley, 1989: On the origin of shelf water in the middle Atlantic bight. *J. Phys. Oceanogr.*, **19**, 384–391, https://doi.org/10.1175/1520-0485(1989)019<0384:OTOOSW>2.0.CO;2.

Connolly, T. P., and S. J. Lentz, 2014: Interannual variability of wintertime temperature on the inner continental shelf of the Middle Atlantic Bight. *J. Geophys. Res. Oceans*, **119**, 6269–6285, https://doi.org/10.1002/2014JC010153.

——, and ——, 2021: Observations of nonlinear momentum fluxes over the inner continental shelf. *J. Mar. Res.*, **79**, 27–66, https://doi.org/10.1357/002224021834614425.

Csanady, G. T., 1978: The arrested topographic wave. *J. Phys. Oceanogr.*, **8**, 47–62, https://doi.org/10.1175/1520-0485(1978)008<0047:TATW>2.0.CO;2.

Edson, J. B., and Coauthors, 2013: On the exchange of momentum over the open ocean. *J. Phys. Oceanogr.*, **43**, 1589–1610, https://doi.org/10.1175/JPO-D-12-0173.1.

Fewings, M. R., and S. J. Lentz, 2010: Momentum balances on the inner continental shelf at Martha's Vineyard coastal observatory. *J. Geophys. Res.*, **115**, C12023, https://doi.org/10.1029/2009JC005578.

Ganju, N. K., S. J. Lentz, A. R. Kirincich, and J. T. Farrar, 2011: Complex mean circulation over the inner shelf south of Martha's Vineyard revealed by observations and a high-resolution model. *J. Geophys. Res.*, **116**, C10036, https://doi.org/10.1029/2011JC007035.

Gobron, K., O. de Viron, G. Wöppelmann, É. Poirier, V. Ballu, and M. Van Camp, 2019: Assessment of tide gauge biases and precision by the combination of multiple collocated time series. *J. Atmos. Oceanic Technol.*, **36**, 1983–1996, https://doi.org/10.1175/JTECH-D-18-0235.1.

Goff, J. A., and Coauthors, 2005: Detailed investigation of sorted bedforms, or "rippled scour depressions," within the Martha's Vineyard coastal observatory, Massachusetts. *Cont. Shelf Res.*, **25**, 461–484, https://doi.org/10.1016/j.csr.2004.09.019.

Grant, W. D., and O. S. Madsen, 1979: Combined wave and current interaction with a rough bottom. *J. Geophys. Res.*, **84**, 1797–1808, https://doi.org/10.1029/JC084iC04p01797.

——, and ——, 1986: The continental-shelf bottom boundary layer. *Annu. Rev. Fluid Mech.*, **18**, 265–305, https://doi.org/10.1146/annurev.fl.18.010186.001405.

Gutierrez, B. T., G. Voulgaris, and P. A. Work, 2006: Cross-shore variations of wind-driven flows on the inner shelf in Long Bay, South Carolina, United States. *J. Geophys. Res.*, **111**, C03015, https://doi.org/10.1029/2005JC003121.

Horwitz, R., and S. J. Lentz, 2014: Inner shelf response to cross-shelf wind stress: The importance of the cross-shelf density gradient in an idealized numerical model and field observations. *J. Phys. Oceanogr.*, **44**, 86–103, https://doi.org/10.1175/JPO-D-13-075.1.

Kenyon, K. E., 1969: Stokes drift for random gravity waves. *J. Geophys. Res.*, **74**, 6991–6994, https://doi.org/10.1029/JC074i028p06991.

Kirincich, A. R., 2013: Long-term observations of turbulent Reynolds stresses over the inner continental shelf. *J. Phys. Oceanogr.*, **43**, 2752–2771, https://doi.org/10.1175/JPO-D-12-0153.1.

——, 2021: Martha's Vineyard Coastal Observatory 2021: State of the observatory report. Woods Hole Oceanographic Institution Rep., 40 pp., https://www.whoi.edu/wp-content/uploads/2021/08/MVCO2021.pdf.

——, and J. A. Barth, 2009: Along-shelf variability of inner-shelf circulation along the central Oregon coast during summer. *J. Phys. Oceanogr.*, **39**, 1380–1398, https://doi.org/10.1175/2008JPO3760.1.

——, and S. J. Lentz, 2017: The importance of lateral variability on exchange across the inner shelf south of Martha's Vineyard, MA. *J. Geophys. Res. Oceans*, **122**, 2360–2381, https://doi.org/10.1002/2016JC012491.

——, ——, J. T. Farrar, and N. K. Ganju, 2013: The spatial structure of tidal and mean circulation over the inner shelf south of Martha's Vineyard, Massachusetts. *J. Phys. Oceanogr.*, **43**, 1940–1958, https://doi.org/10.1175/JPO-D-13-020.1.

Lee, T. N., W. J. Ho, V. Kourafalou, and J. D. Wang, 1984: Circulation on the continental shelf of the southeastern United States. Part I: Subtidal response to wind and Gulf Stream forcing during winter. *J. Phys. Oceanogr.*, **14**, 1001–1012, https://doi.org/10.1175/1520-0485(1984)014<1001:COTCSO>2.0.CO;2.

——, E. Williams, J. Wang, R. Evans, and L. Atkinson, 1989: Response of South Carolina continental shelf waters to wind and Gulf Stream forcing during winter of 1986. *J. Geophys. Res.*, **94**, 10 715–10 754, https://doi.org/10.1029/JC094iC08p10715.

Lentz, S. J., 1993: The accuracy of tide-gauge measurements at subtidal frequencies. *J. Atmos. Oceanic Technol.*, **10**, 238–245, https://doi.org/10.1175/1520-0426(1993)010<0238:TAOTGM>2.0.CO;2.

——, 1994: Current dynamics over the Northern California inner shelf. *J. Phys. Oceanogr.*, **24**, 2461–2478, https://doi.org/10.1175/1520-0485(1994)024<2461:CDOTNC>2.0.CO;2.

——, 2008a: Observations and a model of the mean circulation over the Middle Atlantic Bight continental shelf. *J. Phys. Oceanogr.*, **38**, 1203–1221, https://doi.org/10.1175/2007JPO3768.1.

——, 2008b: Seasonal variations in the circulation of the Middle Atlantic Bight continental shelf. *J. Phys. Oceanogr.*, **38**, 1486–1500, https://doi.org/10.1175/2007JPO3767.1.

——, 2010: The mean along-isobath heat and salt balances over the Middle Atlantic Bight continental shelf. *J. Phys. Oceanogr.*, **40**, 934–948, https://doi.org/10.1175/2009JPO4214.1.

——, 2022: Turbulent thermal-wind-driven coastal upwelling: Current observations and dynamics. *J. Phys. Oceanogr.*, **52**, 2909–2921, https://doi.org/10.1175/JPO-D-22-0063.1.

——, and C. D. Winant, 1986: Subinertial currents on the Southern California shelf. *J. Phys. Oceanogr.*, **16**, 1737–1750, https://doi.org/10.1175/1520-0485(1986)016<1737:SCOTSC>2.0.CO;2.

——, and M. R. Fewings, 2012: The wind-and wave-driven inner-shelf circulation. *Annu. Rev. Mar. Sci.*, **4**, 317–343, https://doi.org/10.1146/annurev-marine-120709-142745.

——, R. T. Guza, S. Elgar, F. Feddersen, and T. H. C. Herbers, 1999: Momentum balances on the North Carolina inner shelf. *J. Geophys. Res.*, **104**, 18 205–18 226, https://doi.org/10.1029/1999JC900101.

Liu, Y., and R. H. Weisberg, 2005: Momentum balance diagnoses for the West Florida Shelf. *Cont. Shelf Res.*, **25**, 2054–2074, https://doi.org/10.1016/j.csr.2005.03.004.

Loder, J. W., B. Petrie, and G. G. Gawarkiewicz, 1998: The coastal ocean of northeastern North America: A large-scale view. *The Global Coastal Ocean: Regional Studies and Syntheses*, A. R. Robinson and K. H. Brink, Eds., *The Sea—Ideas and Observations on Progress in the Study of the Seas*, Vol. 11, John Wiley and Sons, 3–27.

Longuet-Higgins, M. S., 2005: Mass transport in water waves. *Philos. Trans. Roy. Soc.*, **A245**, 535–581, https://doi.org/10.1098/rsta.1953.0006.

Mayer, D. A., 1982: The structure of circulation: MESA physical oceanographic studies in New York bight, 2. *J. Geophys. Res.*, **87**, 9579–9588, https://doi.org/10.1029/JC087iC12p09579.

Moody, J. A., and Coauthors, 1983: Atlas of tidal elevation and current observations on the northeast American continental shelf and slope. U.S. Geological Survey Bulletin 1611, 130 pp., https://pubs.usgs.gov/bul/1611/report.pdf.

Noble, M., B. Butman, and E. Williams, 1983: On the longshelf structure and dynamics of subtidal currents on the eastern United States continental shelf. *J. Phys. Oceanogr.*, **13**, 2125–2147, https://doi.org/10.1175/1520-0485(1983)013<2125:OTLSAD>2.0.CO;2.

Pawlowicz, R., B. Beardsley, and S. Lentz, 2002: Classical tidal harmonic analysis with errors in MATLAB using T_TIDE. *Comput. Geosci.*, **28**, 929–937, https://doi.org/10.1016/S0098-3004(02)00013-4.

Pettigrew, N. R., 1981: The dynamics and kinematics of the coastal boundary layer off Long Island. Ph.D. thesis, Massachusetts Institute of Technology, 262 pp., https://doi.org/10.1575/1912/3727.

Scott, J. T., and G. T. Csanady, 1976: Nearshore currents off Long Island. *J. Geophys. Res.*, **81**, 5401–5409, https://doi.org/10.1029/JC081i030p05401.

Scully, M. E., J. H. Trowbridge, C. R. Sherwood, K. R. Jones, and P. Traykovski, 2018: Direct measurements of mean Reynolds stress and ripple roughness in the presence of energetic forcing by surface waves. *J. Geophys. Res. Oceans*, **123**, 2494–2512, https://doi.org/10.1002/2017JC013252.

Shearman, R. K., and S. J. Lentz, 2004: Observations of tidal variability on the New England Shelf. *J. Geophys. Res.*, **109**, C06010, https://doi.org/10.1029/2003JC001972.

——, and ——, 2010: Long-term sea surface temperature variability along the U.S. East Coast. *J. Phys. Oceanogr.*, **40**, 1004–1017, https://doi.org/10.1175/2009JPO4300.1.

Trowbridge, J., and S. J. Lentz, 2018: The bottom boundary layer. *Annu. Rev. Mar. Sci.*, **420**, 397–410, https://doi.org/10.1146/annurev-marine-121916-063351.

Wang, D. P., 1979: Low-frequency sea level variability on the Middle Atlantic Bight. *J. Mar. Res.*, **37**, 683–696.

Warner, J. C., J. H. List, W. C. Schwab, G. Voulgaris, B. Armstrong, and N. Marshall, 2014: Inner-shelf circulation and sediment dynamics on a series of shoreface-connected ridges offshore of Fire Island, NY. *Ocean Dyn.*, **64**, 1767–1781, https://doi.org/10.1007/s10236-014-0781-y.

Wiberg, P. L., and C. K. Harris, 1994: Ripple geometry in wave-dominated environments. *J. Geophys. Res.*, **99**, 775–789, https://doi.org/10.1029/93JC02726.

Yankovsky, A. E., and R. W. Garvine, 1998: Subinertial dynamics on the inner New Jersey shelf during the upwelling season. *J. Phys. Oceanogr.*, **28**, 2444–2458, https://doi.org/10.1175/1520-0485(1998)028<2444:SDOTIN>2.0.CO;2.